Hindawi
International Journal of Chemical Engineering
Volume 2018, Article ID 3790849, 15 pages
https://doi.org/10.1155/2018/3790849

Research Article

Flame Failures and Recovery in Industrial Furnaces: A Neural Network Steady-State Model for the Firing Rate Setpoint Rearrangement

Tahmineh Adili,[1,2] **Zohreh Rostamnezhad**,[1,2] **Ali Chaibakhsh**,[1,2] **and Ali Jamali**[1]

[1]*Faculty of Mechanical Engineering, University of Guilan, Rasht, Guilan 41938-33697, Iran*
[2]*Intelligent System and Advanced Control Laboratory, University of Guilan, Rasht, Guilan 41938-33697, Iran*

Correspondence should be addressed to Ali Chaibakhsh; chaibakhsh@guilan.ac.ir

Received 8 February 2018; Revised 5 May 2018; Accepted 16 May 2018; Published 20 June 2018

Academic Editor: Konstantinos E. Kakosimos

Burner failures are common abnormal conditions associated with industrial fired heaters. Preventing from economic loss and major equipment damages can be attained by compensating the lost heat due to burners' failures, which can be possible by defining appropriate setpoints to rearrange the firing rates for healthy burners. In this study, artificial neural network models were developed for estimating the appropriate setpoints for the combustion control system to recover an industrial fired-heater furnace from abnormal conditions. For this purpose, based on an accurate high-order mathematical model, constrained nonlinear optimization problems were solved using the genetic algorithm. For different failure scenarios, the best possible excess firing rates for healthy burners to recover the furnace from abnormal conditions were obtained and data were recorded for training and testing stages. The performances of the developed neural steady-state models were evaluated through simulation experiments. The obtained results indicated the feasibility of the proposed technique to deal with the failures in the combustion system.

1. Introduction

Fired heaters are critical units in refineries and petrochemical industries, used for direct heating of a fluid stream in hydrocarbon processing. Hot gases from combustion are directly supplied to the multiple stream tubes by means of convective and radiative heat transfer mechanisms. This considerably increases the temperature of the crude process, which can be fed into distillation columns to be separated into a variety of components [1, 2]. In order to maintain the quality of products, the stream temperature should be controlled. Regulating the firing rate is normally the main tool for achieving target temperature [3].

Nonuniform temperature distribution inside furnaces due to the burners' failures and combustion malfunctions may cause major quality defects in distillation products [4]. The effects of burners' failures may appear in different forms such as flame impingement, flame instability, hot spots, and so on [5]. Ignoring this situation could increase the danger of major equipment damages. Reducing the faulty burner's fuel flow is the main correcting action [6]. In case of failure of a single burner or losing a part of burner firing capacity, the furnace can still continue to function; however, compensating the lost heat to achieve thermal equilibrium would be the main issue. In such circumstances, which are called abnormal conditions, corrective actions should be immediately taken in order to avoid coke formation inside the tubes and consequent possible damages [6, 7].

The strategy to recover the system from abnormal conditions can be characterized by defining appropriate setpoints for the controllers at the lower layer. Integrating expert systems into the monitoring and supervisory control systems has been regarded as a solution to improving the capability of industrial control systems in reacting to unexpected events [8–10]. Such systems should be able to acquire data from instruments, detect and diagnose the

faults, and optimize the process conditions by adjusting new setpoints for control loops to move away from abnormal conditions [11, 12]. Designing an effective expert system usually requires adequate information from the plant variables, real data from critical components conditions, and the knowledge of expert operators about certain abnormal situations [13]. However, the required information from real system performances during the failures of burners is barely in hand. Furthermore, applying artificial failures to in-service fired-heaters to acquire the necessary data is practically impossible [14, 15]. In this case, mathematical models could be employed to investigate the effects of many different failures and firing rate scenarios on heat distribution inside the furnace and optimize the process conditions to cope with abnormal situations [16–18].

Many different model-based optimization techniques have been reported for improving the operation of industrial processes in the literature [19–21]. First-principle models (FPMs) are the common type of steady-state models used for plant monitoring, process optimization, and open-loop decision supports [22]. Due to model uncertainties and disturbances, online steady-state data are required to identify the models. Employing steady-state models could considerably reduce the computational efforts, which is so valuable in real-time optimization (RTO) [23]. Nonlinear mathematical models have been also used for optimizing the operation of industrial processes, which are generally used as the core of nonlinear model predictive control (NMPC) [24, 25].

In recent years, data-based modeling approaches such as artificial neural networks have been widely employed for optimization of industrial processes [18, 26, 27]. The capability of characterizing the behaviors of complicated systems without prior knowledge, low computational costs, and good interpolating performances is the main advantage of neural network models [28]. Different structures of artificial neural networks have been used for optimizing the operation of industrial processes; however, in general, two distinct categories can be identified in their applications: static neural network models are more common in real-time optimization (RTO) applications, whereas steady-state models are required for optimizing the operational conditions at the upper control layers; (2) dynamic neural models are used as the core of model predictive control at the lower control levels [29–31].

In this study, a model-based optimization approach is proposed to find the optimal operational conditions for an industrially fired-heater furnace to be recovered from possible burner failures. A nonlinear mathematical model developed by Chaibakhsh et al. was extended and used for optimization process [32]. Different failure scenarios in the combustion system were applied to the model, and their effects on the tubes and furnace outputs were investigated. Then, constrained nonlinear optimization problems were solved to plan the required excess firing rate for healthy burners to recover from abnormal conditions. The obtained results were employed for training the neural network (NN) estimators. The developed models were used as the core of an abnormal management system (AMS), which was responsible for generating the reference setpoints for the burners' controllers according to the failure situations. The obtained results from the optimization process and the assessment of the effectiveness of the proposed approach were presented for different failure situations.

2. System Description

A cabinet-type, single-firebox furnace shown in Figure 1 is considered for investigation in this study. Five floor-mounted burners are arranged in a row to supply the required heat for convection and radiation sections. The crude process is fed from the top of the furnace and first passes through the convection sections 2 and 1, where its temperature increases from 504.15 K to about 561.65 K, and the fluid often remains as a one-phase liquid. In the radiation section, tubes are exposed to high heat fluxes. The crude process begins with boiling and vaporizing and the temperature increases to about 637 K at the end of this section.

At each wall, the process fluid is divided into two counterflow streams, which are heading to the middle side of the furnace. Each stream also comprises 24 rows of tubes. The required firing rate is about 0.06842 kg/s for each burner at the nominal furnace load of 11.26 kg/s. In Table 1, the nominal parameters of the furnace are presented [32, 33].

An accurate mathematical model was developed by Chaibakhsh et al., which was employed for the optimization process [32]. In order to consider the effects of flame height on the heat absorbed by each tube, the firebox of the fired heater has been divided into five thermal zones, which are shown in Figure 1. The view factor for each subsection of tubes was calculated with respect to their location and the average flame height.

3. Optimization Problem: Objective Function and Genetic Algorithm

In this section, different burners' firing capacity shortage/failure scenarios are applied to the developed model of the furnace. Then, an optimization approach based on the genetic algorithm (GA) was applied to the model in order to find the appropriate firing rate for each burner. The maximum firing rate capacity for each burner, the overall fuel consumption, the tubes' wall temperature, and the furnace outlet temperature are considered as constrains. The procedure of model-based optimization is shown in Figure 2.

3.1. Optimization Problem. The average temperature of two streams (on both sides) is the most important variable that should remain around 637 K (Table 1); this is necessary to achieve the desired product quality and should not be exceeded significantly.

Thus, by defining error as the difference between the average outlet temperature of the crude process and the desired temperature (637 K), the optimum excess firing rate for each burner could be calculated to reduce the outlet temperature errors, according to the constraints on variables.

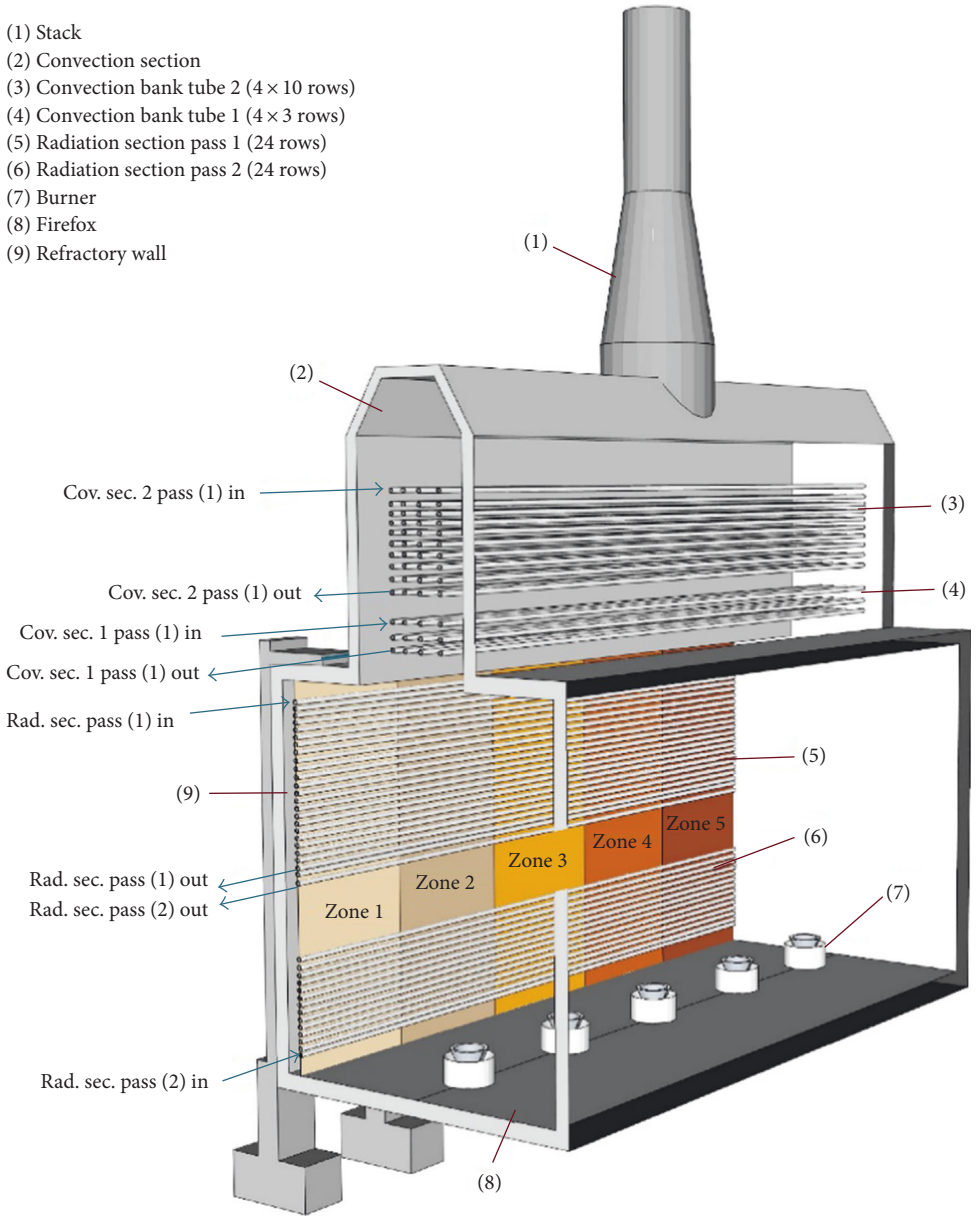

Figure 1: Schematic of the fired-heater furnace.

The objective function for the optimization process can be defined as follows:

$$\min J_{\dot{m}_{\text{fuel}}} = \int_{t=t_0}^{t=t_f} \gamma\left(T_{\text{oil}}(t), T_{\text{tube}}(t), \dot{m}_{\text{fuel}}, \dot{m}_{\text{oil}}\right)dt, \quad (1)$$

where T_{oil} and T_{tube} denote the state variables oil and tube surface temperature, respectively. In addition, $\dot{m}_{\text{fuel}}$ and $\dot{m}_{\text{oil}}$ are fuel and crude process flow rates fed to the furnace, respectively. This objective function is used for each zone of each tube, and the optimization process is performed for all abnormal conditions, which may occur during systems operation. The considered functions for the optimization problem definition are as follows:

$$\frac{dT_{\text{tube}_k}}{dt}(i,j) = \Psi_k\left(T_{\text{oil}_{\text{in}}}(i,j), T_{\text{oil}_{\text{out}}}(i,j), T_{\text{tube}}(i,j), F(i,j), \dot{m}_{\text{fuel}}, u_1\right), \quad i = 1,2,\ldots,24,\ j = 1,\ldots,5,\ k = 1,\ldots,4. \quad (2)$$

The function of the tube's temperature in the radiation section is presented in (2), whereas the following equation shows the relation between crude process's temperature and the heat absorbed from the tubes:

Table 1: The nominal parameters of the furnace.

Parameter (unit)	Symbol	Value
Process fluid flow rate (kg/s)	$\dot{m}_{in}$	45
Process fluid inlet temperature (K)	T_{in}	504
Process fluid outlet temperature (K)	T_{out}	637
Process fluid inlet pressure (kPa)	P_{in}	1036
Process fluid outlet pressure (kPa)	P_{out}	371
Fuel flow rate (kg/s)	$\dot{m}_{\text{fuel}}$	0.07
Tube out diameter (m)	D_{out}	0.12
Tube wall thickness (m)	Δr	0.012
Process fluid outlet temperature at convection section 2 (K)	$T_{\text{out-convection 2}}$	544
Process fluid outlet temperature at convection section 1 (K)	$T_{\text{out-convection 1}}$	562
Process fluid outlet pressure at convection section 2 (kPa)	P	823
Process fluid outlet pressure at convection section 1 (kPa)	P	772
Fuel gas lower heating value (MJ/kg)	LHV	48.594
Tube length (m)	L	3.4
Mean gas-side heat transfer coefficient in convection section 2 (w/m^{2}K)	h_{gas}	238.5
Mean gas-side heat transfer coefficient in convection section 1 (w/m^{2}K)	h_{gas}	277
Mean oil heat transfer coefficient in convection section 2 (w/m^{2}K)	h_{oil}	4871
Mean oil heat transfer coefficient in convection section 1 (w/m^{2}K)	h_{oil}	3737
Mean gas-side heat transfer coefficient in the radiation section (w/m^{2}k)	h_{gas}	548
Furnace height (m)	—	12.5
Furnace depth (m)	—	5.5
Furnace width (m)	—	5.2
Number of passes in convection and radiation sections	—	4
Number of rows of tubes in convection section 2	—	10
Number of rows of tubes in convection section 1	—	3
Number of tubes in one pass of the radiation section	—	24

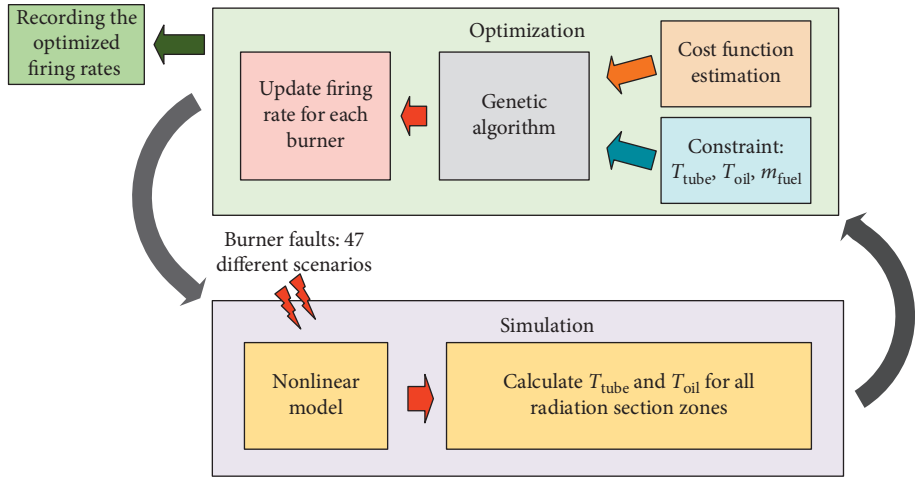

Figure 2: Procedure of the optimization problem for obtaining the appropriate firing rates.

$$\frac{dT_{\text{oil}_k}}{dt}(i,j) = \Phi_k\left(T_{\text{oil}_{\text{in}}}(i,j), T_{\text{oil}_{\text{out}}}(i,j), T_{\text{tube}}(i,j), \dot{m}_{\text{oil}}, u_2\right), \quad i = 1,2,\ldots,24,\ \ j = 1,\ldots,5,\ \ k = 1,\ldots,4. \tag{3}$$

In the convection section, (4) is used for estimating the tube's temperature, and (5) is the crude process's temperature function:

$$\frac{dT_{\text{tube}_k}}{dt}(i) = \Gamma_k\left(T_{\text{oil}_{\text{in}}}(i), T_{\text{oil}_{\text{out}}}(i), T_{\text{tube}}(i), \dot{m}_{\text{fuel}}, u_3\right), \quad i = 1,2,\ldots,13,\ \ k = 1,\ldots,4, \tag{4}$$

$$\frac{dT_{\text{oil}_k}}{dt}(i) = \Omega_k\left(T_{\text{oil}_{\text{in}}}(i), T_{\text{oil}_{\text{out}}}(i), T_{\text{tube}}(i), \dot{m}_{\text{oil}}, u_4\right), \quad i = 1,2,\ldots,13,\ \ k = 1,\ldots,4. \tag{5}$$

In addition, a limitation is considered on the excess firing rate for each burner as follows:

$$0 \le \dot{m}_{\text{fuel}_j} \le \dot{m}_{\text{fuel,max}}, \quad j = 1, 2, \ldots, 5. \tag{6}$$

The maximum tube design temperature is restricted as

$$T_{\text{tube}}(i, j) \le T_{\max}. \tag{7}$$

The inputs and outputs of all passes are located in Zone 1; accordingly, the process output temperature T_k would be calculated as

$$T_k = T_{\text{oil}_k}(24, 1), \quad k = 1, \ldots, 4. \tag{8}$$

In case of failure in a burner, heat loss should be compensated by increasing the firing rate in the other burners. It should be noted that the furnace's thermal zones would change due to any variation in flame height. In order to determine the heat absorbed by each section of the tubes, the view factor for each subsection of tubes should be calculated with respect to their location and the average flame height. The geometric description for the tube and flame and the effects of flame's height on the view factors are presented in Appendix. Increasing the temperature of tube surfaces is the most significant effects of overfiring, which should be limited due to its critical effects on the safety of the furnace. The maximum tube design temperature is about 900 K; however, increasing the surface temperature of the tube could increase the danger of coke formation and internal tube fouling. Therefore, the maximum target surface temperature is considered to be 800 K as follows:

$$T_{\text{tube}}(i, k) - 800 \le 0, \quad i = 1, 2, \ldots, 24, \; k = 1, \ldots, 4. \tag{9}$$

The appropriate firing rate for each burner can be measured by solving the nonlinear optimization problem in the form of (2) to (5) subject to inequality constrains of (6) and (7) using the genetic algorithm. In order to keep solutions in the feasible region, it is required to convert a constrained optimization problem to an unconstrained optimization [34]. Employing penalty functions are a common approach to dealing with constrains in solving nonlinear optimization problems by GA. It is applied as follows:

$$P_{i,j} = \begin{cases} 0, & T_{\text{tube}}(i, j) < 800, \\ \dfrac{T_{\text{tube}}(i, j)}{800} - 1, & T_{\text{tube}}(i, j) \ge 800, \end{cases} \tag{10}$$
$$i = 1, 2, \ldots, 24, \; j = 1, \ldots, 5.$$

The penalty function P_{S_k} is simplified for the stream k as

$$P_{S_k} = \frac{1}{2}\left[\left(\frac{T_{\max S_k}}{800} - 1\right) + \left|\frac{T_{\max S_k}}{800} - 1\right|\right], \quad k = 1, \ldots, 4, \tag{11}$$

where $T_{\max S_k}$ is the maximum surface temperature of tubes (24 passes for each stream pass) and is given as

$$T_{\max S_k} = \max\left(T_{\text{tube}}(i, j)\right)_k, \quad i = 1, 2, \ldots, 24, \; j = 1, \ldots, 5, \; k = 1, \ldots, 4. \tag{12}$$

The penalty functions could prevent the tubes' surface temperature from reaching the maximum values. They have a zero value if the surface temperature is less than the maximum value. By excessing the considered limit, the penalty function would have a nonzero (positive) value, which could be magnified by considering a large value for penalty constant α.

$$P_S = \max\left(P_{S_k}\right), \quad k = 1, \ldots, 4. \tag{13}$$

In order to compensate for the heat loss due to burner failures, the sum of excess mass flow rates in healthy burners should be equal to the missed flow rates in faulty burners. However, by increasing the burners' firing rate, the heat transfer performance will increase. Therefore, this value could be a little (about 3 percent) less than the required amount. The maximum value of excess firing rate is also limited to 30 percent. It is applied by

$$-0.03 \le \sum \dot{m}_{\text{fuel}_{\text{exceed}}} - \dot{m}_{\text{fuel}_{\text{loss}}} \le 0.3. \tag{14}$$

The penalty function for limiting the excess fuel flow rate can be defined through the following equation:

$$P_{\text{fuel}} = \frac{1}{2}\left\{\left[\left(\frac{\sum \dot{m}_{\text{fuel}_{\text{exceed}}}}{1.2\sum \dot{m}_{\text{fuel}_{\text{loss}}}} - 1\right) + \left|\frac{\sum \dot{m}_{\text{fuel}_{\text{exceed}}}}{1.2\sum \dot{m}_{\text{fuel}_{\text{loss}}}} - 1\right|\right] + \left[\left(1 - \frac{\sum \dot{m}_{\text{fuel}_{\text{exceed}}}}{0.97\sum \dot{m}_{\text{fuel}_{\text{loss}}}}\right) + \left|1 - \frac{\sum \dot{m}_{\text{fuel}_{\text{exceed}}}}{0.97\sum \dot{m}_{\text{fuel}_{\text{loss}}}}\right|\right]\right\}. \tag{15}$$

The penalty function, P_{fuel}, is considered for economical operation, and the optimization process is performed based on reducing fuel consumption. However, in case of the failure/firing capacity shortage of two burners, it is not economically justifiable. In these cases, the burner's firing rate may be close to their maximum capacity, meaning that the total fuel flow rate might be more than its amount in normal operating conditions.

As a result, the fitness function is defined as

$$f = \left|\sum_{k=1}^{2}\left(T_k - 637\right)\right| + \left|\sum_{k=3}^{4}\left(T_k - 637\right)\right| + \alpha P_s + \beta P_{\text{fuel}}, \quad (16)$$

where $P(.)$ is a penalty function and α and β are penalty constants. This is a constrained optimization problem, which was transformed to an unconstrained one using an additive penalty function $P(.)$ [34].

3.2. Genetic Algorithm (GA). Genetic algorithm (GA) methodologies have been investigated as efficient approaches for obtaining solutions very close to optimum points [35, 36]. GA is a nongradient-based stochastic technique, which is capable of exploring and exploiting the search space for the optimal solution. The GA operators including crossover and mutation allow the searching algorithm to escape from possible local minima trapping points. In addition, it is very robust to dynamic changes in the environment. This advantage has made it an appropriate tool for the optimization of systems working under different operating conditions with different behaviors [37]. Different applications of GA were reported for designing decision-making systems based on nonlinear optimization problems [38].

The optimization processes were performed by using MATLAB® Optimization Toolbox (The MathWorks, Inc., Natick, MA, USA, ver. 2014). An appropriate selection of GA parameters could improve the performance of algorithm and reduce the runtime considerably [39]. Crossover is a recombination operator that could generate better offspring through generations by selecting randomly a pair of two individuals, choosing a cross site along the string length and finally swapping between the two strings following the cross site. After creation of new individuals via crossover, mutation is applied usually with a low probability to introduce random changes into the population [37]. Generally, the crossover rate of about 80 to 90% should be chosen. However, some results show that for some problems the crossover rate of about 60% is the best. The mutation rate should be very low, and it is reported that the best rates is about 0.5 to 1%. The proper values of crossover and mutation rates can be chosen by performing some experiments to find the best solution. It is possible to estimate the optimal population sizes based on some analytic methods on particular problems [37]. However, a default population size of about 20 to 30 is adequate to find the optimal solution; however, sometimes it has been reported that the size of 50 to 100 could be the best. Elite selection is the strategy to choose individuals with a best fitness value to pass to the next generation. The selection could be performed randomly according to the limited elites. In Table 2, the parameters for optimization by the GA are presented.

Table 2: The optimization parameters for GA.

Population size	100
Crossover rate	0.7
Mutation rate	0.02
Generations	100
Migration	Forward, fraction: 0.2, int.: 20
Selecting	Stochastic uniform
Reproduction	Elite count: 5

4. Neural Network Model

A multilayer perceptron (MLP) structure was considered for the neural network (NN) model. MLP is a feedforward neural network (FFNN), which can be used for characterizing complex relationships between variables and predicting future values in a process. MLP has a set of layers (including input, hidden, and output layers) and computational units (activation function), which are related to the layers' node by weight coefficients. Generally, one or more hidden layers can be considered in MLP; however, a single hidden layer might be adequate to reach an acceptable degree of accuracy in many cases [40, 41].

The number of neurons, as a dominant parameter in the model performances, was considered with respect to the number of input/output variables. Azoff recommended that the number of neurons at the hidden layer (N_h) for a single hidden layer NN be chosen as follows:

$$N_h = 2 \times N_u + 1, \quad (17)$$

where N_u is the number of network inputs [42]. In order to adjust the parameters of models, the second-order derivative-based Levenberg–Marquardt (LM) was employed. The LM is a common algorithm for training the parameters of moderate-size MLPs. The mean square of error (MSE) was used as the objective function for the training process, which should be minimized as follows:

$$e = \frac{1}{p}\sum_{i=1}^{p}\left(y_i^* - y_i\right)^2, \quad (18)$$

where y_i^* and y_i are the target and actual outputs for the ith pattern, respectively, and p is the total number of training patterns. The error vector E is calculated as follows:

$$E = \left[e_1, e_2, e_3, \ldots, e_p\right]^T. \quad (19)$$

For the set of the considered inputs, x_P, the output neurons, y_k, are calculated through the following equation:

$$y_{k,p} = f_{yk}\left(\sum_{j=1}^{N_h} w_{kj} f_{hj}\left(\sum_{i=1}^{N_u} w_{ji} x_{i,p}\right)\right), \quad (20)$$

where f_{yk} and f_{hj} are transfer functions related to output neurons, k, and hidden neurons, j, respectively; also, w_{kj} is the weights interface between the kth output neurons and the jth hidden neurons, and w_{ji} is the jth hidden neuron and the ith input neuron.

5. Failure Scenarios: Optimizations and Setpoints

In this section, 47 different constrained optimization problems were solved in order to obtain the appropriate firing rate for the burners in different failure scenarios. The

developed model for the furnace employed for optimization is a continuous state model. The firing rates are discrete variables that are selected by the GA, and then, the equations are solved in order to obtain the temperatures of tubes and outlets of all passes. In the considered furnace, each burner has its individual control valve, which allows a considerable excessive firing rate up to 30 percent of the nominal firing rates for each burner. In this case, the heat loss due to a single burner failure or firing shortage in two or three burners may be compensated. For investigating the possibility of recovering the furnace from abnormal conditions, many different cases are considered. The failure scenarios applied to the burners are discrete variables. The simulation experiments and optimization are preformed while the available firing capacities are at 75, 50, and 25 percent of the nominal firing rates and also in the case of complete burner failures. The firing capacity of burners can be estimated by the measured mass flow rate of the fuel fed to each burner. It should be noted that no control actions should be applied during optimization stages.

It should be noted that the results are achieved through time-consuming optimization processes using a high-order nonlinear model; therefore, only a limited number of failure scenarios could be investigated. The model employed for optimization processes was a model with 1064 states (ODE equations), where the runtime for each optimization process using a PC with Intel® Core™ i7 4510U @2.60 GHz, RAM 8.00 GB, and a operating system Windows® 8.1 (x64) was about 24 hours.

5.1. Model Responses and Optimization Results. Exposure to various disturbances, unplanned variations in the process flow rate, and changes in fuel components or pressure drop could affect the operating conditions and thermal performances of preheat furnaces [5, 43]. Useful information on the load pattern can be obtained from simulation experiments using the developed model. This can be used in designing the expert furnace supervisory control and burner management systems in order to achieve the desired outlet process temperature at different operating conditions.

Figure 3(a) shows the crude process outlet temperature versus the fuel flow rate as the process flow changes. The required firing rate for burners to achieve desired process temperature of 637 K, at different process loads is shown. This value is about 0.06842 kg/s for each burner at the nominal furnace load of 11.26 kg/s. The changes in the process flow rate have considerable effects on the outlet temperature at a constant firing rate. For this reason, the process flow rate is considered as the main manipulated variable for regulating the outlet temperature of each path, and a control valve is supplied at the inlet of the individual path to the radiation section.

In Figure 3(b), the temperature differences of two stream passes are presented. The obtained results indicate that, by increasing the fuel flow rate, the outlet temperature difference between passes 1 and 2 would reach its maximum values as the total fuel flow rate exceeds up to 10 percent over the nominal firing capacity. By increasing the firing rate, the temperature difference starts to reduce again. With respect to the position of each pass in the furnace, the changes in the firing rate could affect the flame height, and consequently, the view factor between the flame and tube passes, which could cause a significant difference between the outlet temperatures of two stream passes. Reducing the temperature difference could improve the energy balance and result in much stable conditions inside the furnace. Some refineries try to increase their productivity by pushing the plant to its overdesign limits, which can be achieved by excessive firing. This limit for fired heaters is often 20 percent in normal operating conditions [6]. In this case, the difference in temperature of stream passes would be small; however, excessive firing capacity may not be adequate to compensate for the effects of burner failures. Thus, the proposed method could be applicable, if the furnace is run in its nominal design conditions.

Figure 3(c) presents the tube surface temperature versus the fuel flow rate at different furnace loads. A decrease in the process load causes the heat absorbed by the crude process to decrease and consequently the tube surface temperature to increase significantly, which is not desirable. The tube temperature is a critical variable that should not be tolerated from its acceptable range. The tube surface temperature does not normally reach its limit until the process fluid flows inside the tubes (Figure 3(c)). Continuous flame impingement on the tubes is the main potential problem that may occur and lead to coke formation and early furnace failure. The risk of tubes' surface localized overheating in places where no tube-skin thermocouple is installed is especially high. Generally, flame impingement can be discovered only by visual observation and should be avoided by any means possible. Localized overheating more than 38°C above the designed temperature of tubes would be the cause for their failure in a matter of hours [7]. In this case, the operator could make the flame lean away from the tubes by pulling the flame down [6]. However, this could significantly deteriorate the performance of the furnace, which should be compensated by excess firing of the remaining healthy burners.

The main reason for choosing the genetic algorithm was its capability to search for best results in a global searching space. Despite it being a little slow for the high-order system to capture the optimum points, it would ensure the obtained results are global optimum solutions. By performing constrained optimization based on the GA, the best possible firing rate for each burner was obtained. Table 3 presents the required excess firing rate for healthy burners and the outlet temperature deviations as one burner fails (20 cases). Process flow enters the furnace at the front side and leaves it from the same side. Hence, the effects of failures in burners 1 or 5 and burners 2 or 3 would be considerably different in the outlet temperature. The maximum temperature deviations can be observed as the burners 1 and 5 fail; however, the failure of burner 1, the nearest burner to the front wall, can be recognized as the worst case. In these cases, excess firing rate reaches its maximum capacity of burners, and any further attempts to reduce the temperature deviations increase the risk of tubes overheating. This causes a small reduction in the total fuel flow rate.

When the burners that are closer to the center be faulty, the temperature deviations were considerably reduced. The obtained results showed that the furnace could certainly be

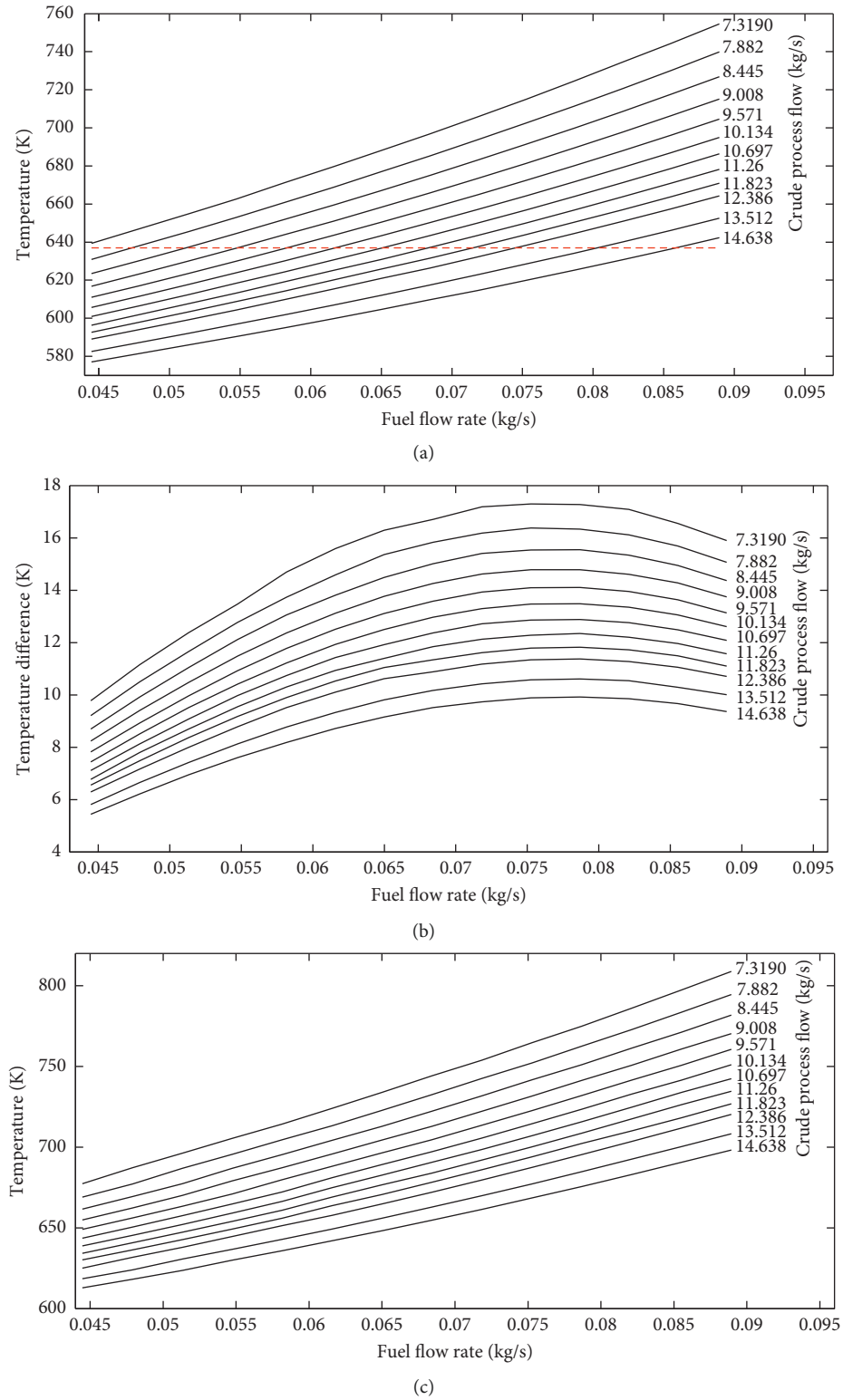

Figure 3: (a) Crude process temperature versus fuel flow rate. (b) The temperature difference of passes versus fuel flow rate. (c) Tube surface temperature versus fuel flow rate.

recovered from abnormal conditions. However, a small increase in the fuel flow rate could be observed, making it economically less desirable. Despite the effectiveness of the proposed approach in dealing with faulty burners, due to economic reasons and also a high thermal stress, the furnace could not run for a long time in such conditions.

The required firing rates for healthy burners to recover the heat balance inside the furnace as two faulty burners operate at

Table 3: Single-burner failure/firing capacity shortage.

	Burner 1 excess flow (%)	Burner 2 excess flow (%)	Burner 3 excess flow (%)	Burner 4 excess flow (%)	Burner 5 excess flow (%)	Temperature deviation (K)	Total fuel flow rate changes (%)
Case 1	*Fail*	27.74	23.79	24.23	23.79	3.8	−0.45
Case 2	*25% capacity*	23.5	19.99	21.45	16.49	0.014	+6.43
Case 3	*50% capacity*	19.99	12.69	14.44	10.64	0.006	+7.76
Case 4	*75% capacity*	10.49	8.44	9.03	7.28	0.006	+10.24
Case 5	27.74	*Fail*	24.38	23.79	23.65	3.1	−0.44
Case 6	22.19	*25% capacity*	19.12	17.51	18.82	0.011	+2.64
Case 7	17.22	*50% capacity*	16.19	8.31	11.22	0.002	+2.94
Case 8	10.34	*75% capacity*	8.89	4.50	6.40	0.002	+5.13
Case 9	24.38	26.42	*Fail*	27.00	23.79	1.81	+1.59
Case 10	15.32	22.19	*25% capacity*	21.89	15.61	0.002	+0.01
Case 11	9.91	15.61	*50% capacity*	16.05	9.62	0.001	+1.19
Case 12	5.22	9.47	*75% capacity*	8.74	4.91	0.001	+3.34
Case 13	23.65	23.79	24.38	*Fail*	27.74	2.71	−0.44
Case 14	17.81	16.63	18.53	*25% capacity*	21.63	0.011	+0.6
Case 15	10.77	8.00	15.91	*50% capacity*	16.64	0.003	+1.32
Case 16	6.11	4.21	8.74	*75% capacity*	9.91	0.001	+3.97
Case 17	23.79	24.08	23.65	27.59	*Fail*	2.8	−0.89
Case 18	15.02	20.00	18.53	22.04	*25% capacity*	0.013	+0.59
Case 19	9.18	12.98	11.22	18.53	*50% capacity*	0.006	+1.91
Case 20	5.82	7.57	6.99	9.03	*75% capacity*	0.0021	+4.41

Table 4: Two-burner failure/firing capacity shortage.

	Burner 1 excess flow (%)	Burner 2 excess flow (%)	Burner 3 excess flow (%)	Burner 4 excess flow (%)	Burner 5 excess flow (%)	Temperature deviation (K)	Total fuel flow rate changes (%)
Case 21	*50% capacity*	*50% capacity*	28.03	26.43	27.1	7.94	−18.44
Case 22	*75% capacity*	*75% capacity*	23.36	19.70	21.02	0.23	+14.08
Case 23	*50% capacity*	28.03	*50% capacity*	27.12	26.15	4.9	−18.7
Case 24	*75% capacity*	22.75	*75% capacity*	17.07	16.04	0.1	+5.86
Case 25	*50% capacity*	28.14	26.35	*50% capacity*	27.14	8.1	−18.37
Case 26	*75% capacity*	22.08	16.68	*75% capacity*	19.01	0.31	+7.77
Case 27	*50% capacity*	28.03	26.15	28.33	*50% capacity*	9.01	−17.49
Case 28	*75% capacity*	22.21	17.95	21.02	*75% capacity*	0.81	+11.18
Case 29	28.33	*50% capacity*	*50% capacity*	27.45	26.72	4.37	−17.5
Case 30	17.81	*75% capacity*	*75% capacity*	17.1	15.32	0.11	+0.23
Case 31	27.97	*50% capacity*	27.02	*50% capacity*	28.03	3.21	−16.98
Case 32	18.32	*75% capacity*	15.89	*75% capacity*	17.36	0.11	+1.57
Case 33	27.15	*50% capacity*	26.02	28.03	*50% capacity*	3.5	−18.8
Case 34	16.23	*75% capacity*	14.73	19.71	*75% capacity*	0.091	+0.67
Case 35	26.57	27.45	*50% capacity*	*50% capacity*	28.33	3.01	−17.65
Case 36	14.88	16.78	*75% capacity*	*75% capacity*	17.22	0.09	−1.12
Case 37	26.14	27.1	*50% capacity*	28.03	*50% capacity*	3.38	−18.73
Case 38	13.76	15.37	*75% capacity*	21.00	*75% capacity*	0.09	+0.13
Case 39	27.1	26.13	28.03	*50% capacity*	*50% capacity*	3.7	−18.74
Case 40	15.32	13.71	21.00	*75% capacity*	*75% capacity*	0.1	+0.03
Case 41	*75% capacity*	*50% capacity*	28.03	26.3	27.09	2.98	+6.42
Case 42	*50% capacity*	*75% capacity*	28.12	26.45	27.16	3.7	+6.73
Case 43	24.98	*75% capacity*	*50% capacity*	25.38	23.96	0.11	−0.68
Case 44	23.86	25.00	*50% capacity*	*75% capacity*	24.01	0.019	−2.13
Case 45	24.99	24.16	25.86	*75% capacity*	*50% capacity*	0.09	+0.01
Case 46	24.73	23.92	25.48	*50% capacity*	*75% capacity*	0.089	−0.87
Case 47	*50% capacity*	28.33	26.19	28.03	*75% capacity*	4.96	+7.55

a lower capacity than their nominal firing capacities are given in Table 4. Here, 27 different cases are presented as examples (they are more than 40 cases). The obtained results indicate that the heat loss can be compensated by healthy burners as two faulty burners run at 75 percent of their firing capacity. However, this causes a significant increase in the total fuel flow

Table 5: Fuel flow rate changes versus furnace load for economic operation evaluation.

Process load (kg/s)	Process load changes (%)	Fuel flow rate (kg/s)	Fuel flow rate changes (%)	Tube surface temperature (K)	Efficiency (%)
7.3190	−35	0.04351	−36.4075	674.5	74.32
7.882	−30	0.04742	−30.6928	675.9	75.49
8.445	−25	0.05126	−25.0804	677.1	76.47
9.008	−20	0.05489	−19.77	679.4	77.27
9.571	−15	0.05839	−14.659	680.4	77.94
10.134	−10	0.06182	−9.6463	681.6	78.53
10.697	−5	0.06519	−4.7208	683	79.05
11.26	Nominal	0.06842	Nominal	683.9	79.5
11.823	+5	0.07161	+4.6624	685.4	79.9
12.386	+10	0.07465	+9.1055	685.9	80.25
12.949	+15	0.07751	+13.2856	687.1	80.56
13.512	+20	0.08038	+17.4803	688.5	80.84
14.075	+25	0.08321	+21.6165	690	81.1
14.638	+30	0.08594	+25.6065	691.4	81.34

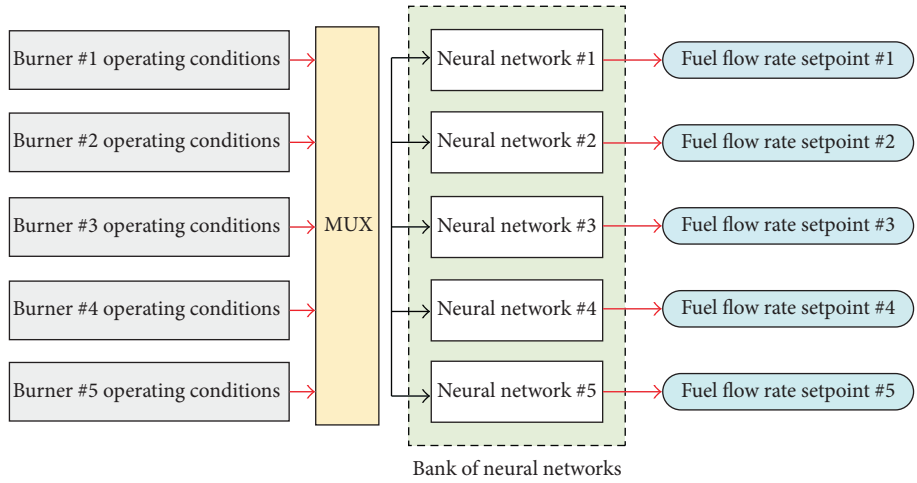

Figure 4: Structure of the neural network model.

rate. When the faulty burners are located at the front side of the furnace the total fuel flow rate increases by about 14 percent. This means that a large amount of energy is wasted in long-term operations of the furnace. Conditions labeled as "Case 41" to "Case 47" are associated with cases that one faulty burner runs at 75 percent while the second one only has a half firing capacity. As presented in Table 4, regarding the faulty burners located at the two ends of the furnace, despite the considerable excess fuel flow rate, still a large deviation in outlet temperature can be observed. Such large outlet temperature changes may deteriorate the quality of distillation products.

The outlet temperature deviations reach their maximum values as the firing capacity of two burners reduced by 50 percent (Table 4). In these cases, considerable decreases in the total fuel flow rate can be observed, and it is clear that it is impossible to recover the furnace from abnormal conditions. For more than two faulty burners (e.g., three burners with 75 percent of firing capacity), it is impractical to recover the furnace to continue its operation at nominal load. In such cases, the furnace should inevitably be shut down or run under lower load conditions. In Table 5, the required fuel flow rates associated with the furnace load at different conditions are presented. As can be seen, there are no considerable changes in the fuel/load ratio. This allows dealing with abnormal situations by reducing the process load.

It should be noted that running fired-heater furnaces at low load conditions is not economically affordable, due to huge energy waste in the upstream and downstream units [7]. In addition, by reducing the crude process flow rate, the fouling rate would increase inside the tubes [44].

5.2. Steady-State Model: Training and Validation. The obtained data from the optimization process were employed to develop the NN model as the core of the abnormal management system (AMS). The structure of the proposed system is shown in Figure 4, in which a bank of multi-input-single-output (MISO) models are employed as the reference estimators. For each burner, an individual MLP model with five inputs and one output was considered. The firing capacity of burners, which is defined as the ratio of actual fuel flow rates to its nominal values, was employed as the models'

Table 6: The performances of the developed neural network estimator.

	NN model	Burner 1	Burner 2	Burner 3	Burner 4	Burner 5
R^2	Train	0.9997	0.9991	0.9969	0.9999	0.9991
	Test	0.9931	0.9992	0.9901	0.9944	0.99601
	Validation	0.9941	0.9943	0.9975	0.9987	0.9921
MSE	Train ($\times 10^{-5}$)	7.3233	3.2427	3.99622	36.274	73.379
	Test ($\times 10^{-4}$)	6.3474	17.91	22.217	6.1263	11.521
	Validation ($\times 10^{-4}$)	0.11646	24.157	17.34	51.057	34.751

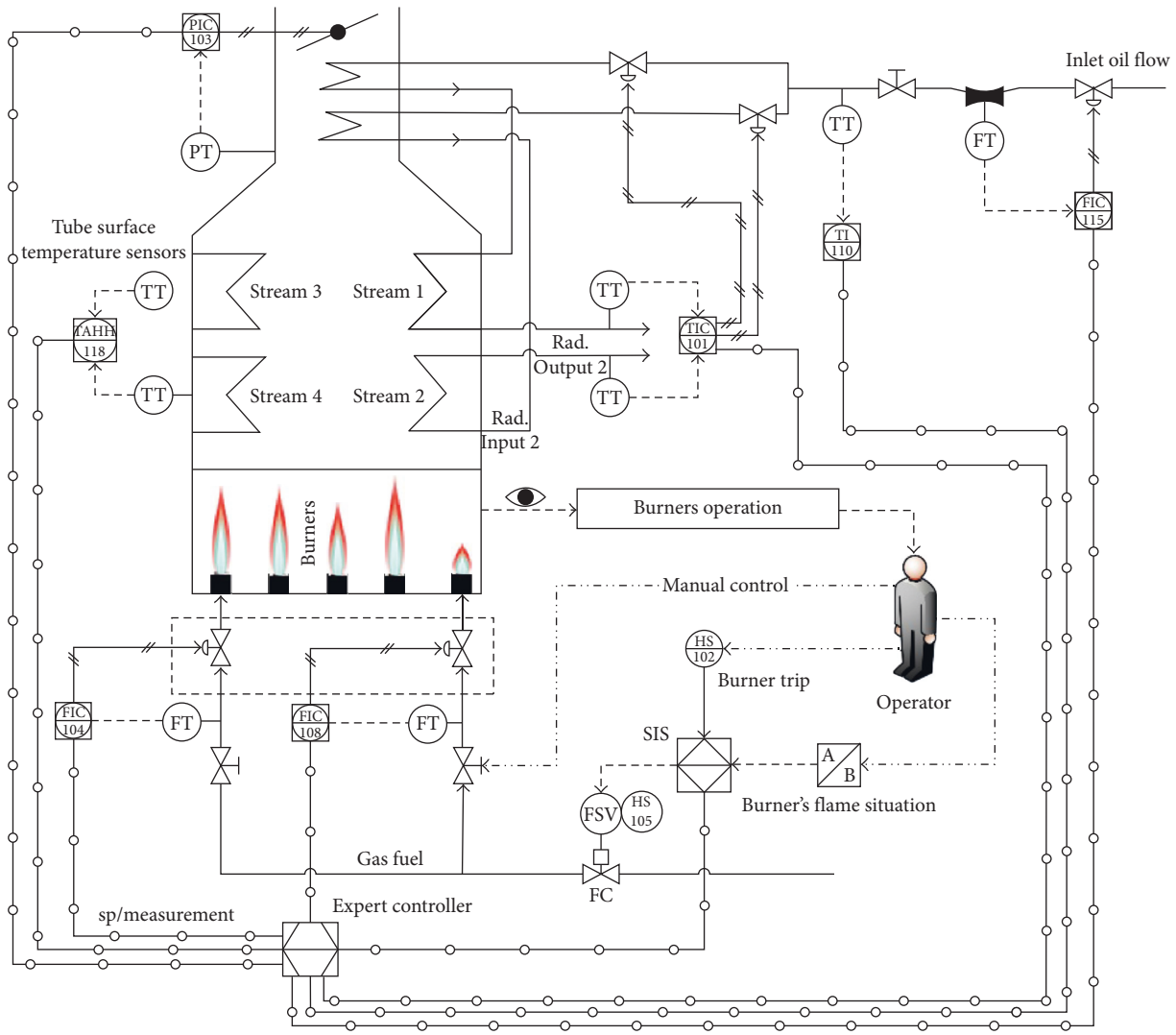

Figure 5: A schematic of control system configuration for a fired-heater furnace unit.

inputs ($x \in [0, 1]$). The corrective positions for control valves were also considered as the models' output ($y \in [0, 1.3]$). The number of neurons in the hidden layer N_h, based on (17), would be equal to 11. The data were collected for 47 data points, which are divided into training (70%), testing (15%), and validation (15%) subsets.

In order to assess the performances of the developed models, the coefficient of determination (R^2) and mean square error (MSE) are employed, as shown below:

$$R^2 = \left(1 - \frac{\sum_{i=1}^{n} \left(y_i^* - y_i^{(i)}\right)^2}{\sum_{i=1}^{n} \left(y_i^* - \overline{y}\right)^2}\right),$$
$$\text{MSE} = \frac{1}{n} \sum_{i=1}^{n} \left(y_i^* - y_i\right)^2, \tag{21}$$

where $\overline{y}$ is the average of y over the n data, and y_i^* and $y_p^{(i)}$ are the ith target and predicted responses, respectively.

The performances of the developed models are presented in Table 6.

The developed neural networks were employed to rearrange the setpoints for the burners' control system based on the detected failures. The developed NN model could estimate the reference setpoints for each burner by interpolating the untrained inputs in new situations.

5.3. Simulation Experiments. In order to evaluate the performances of the proposed control system, simulation experiments were carried out in MATLAB Simulink environments. A schematic of the furnaces control systems is presented in Figure 5. With the occurrence of an event, for example, flame impingement, the corrective action by the operator is to reduce the flame height. In this case, the controller could automatically set the appropriate desired flow rate for other healthy burners to recover the furnace from abnormal conditions. By measuring the actual fuel flow rates, the corrective actions can be estimated by a bank of neural network models in order to compensate for the heat balance inside the furnace.

The operator is able to shut off the burners by a trip command or can set new setpoints for flow controllers from the control panel. Manual closing of the valves or controlling the fuel flow rate for burners in the field can be also detected by the control system. In case of abnormal situations or burner failures, the control system would be able to response appropriately to the new conditions. In Figure 6(a), the responses of the system, as burner #3 loses 80% of its nominal heat capacity, are presented.

This example shows that the AMS is able to detect the fault immediately after its occurrence and modify the burner's valve position, as shown in Figure 6(b). The obtained results indicate the feasibility and effectiveness of the developed controller in dealing with abnormal conditions.

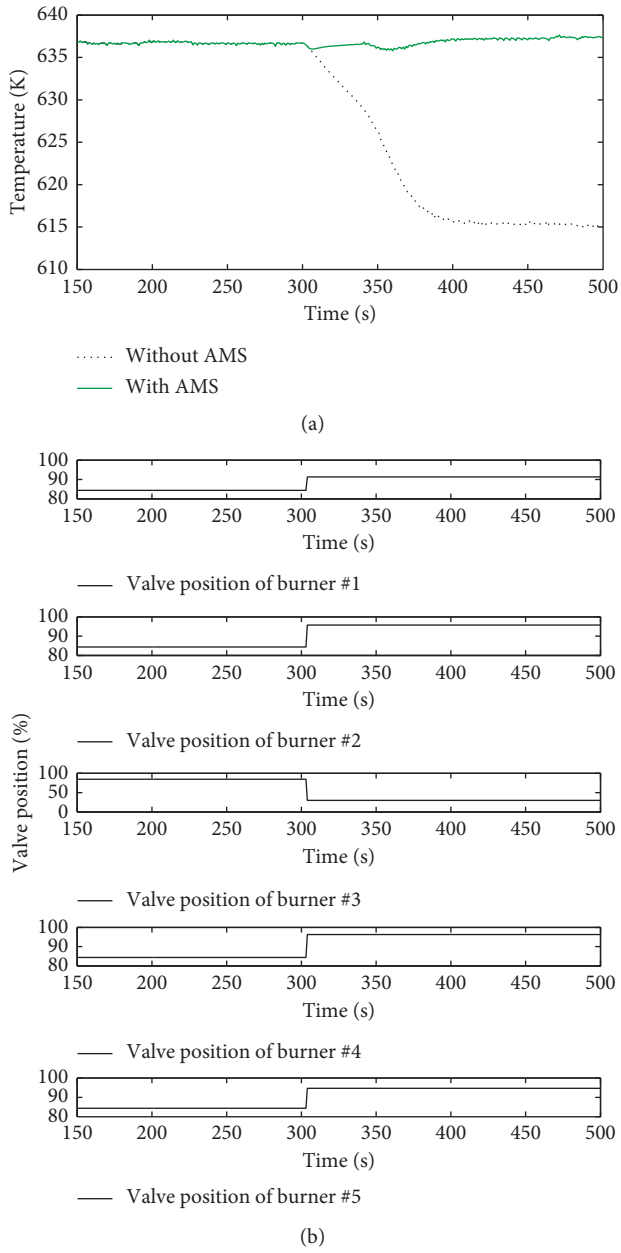

Figure 6: (a) Simulation result of the system. (b) Burner's valve positions response when burner 3 lost 80% of its nominal heat capacity.

6. Conclusion

In this study, steady-state neural network models were developed for estimating the fuel flow rate setpoints for the combustion control system to recover an industrially fired-heater furnace from abnormal conditions. Constrained nonlinear optimization problems were solved using the genetic algorithm to find appropriate firing rates for healthy burners to compensate the heat losses due to failures, where the recorded data are used for training the NN models. The performances of the proposed system were evaluated at different burners' failure situations. The obtained results indicate the applicability of a model-based optimization approach to find the required firing rate for recovering the furnace from abnormal conditions. This provides conceptual basis for designing real-time abnormal management systems (AMS) for fired-heater furnaces.

The steady-state neural models can be used in real-time optimization in order to improve the operational performance of control systems. By considering the economic indices, the developed neural network models can be also employed as the core of economic model predictive controllers (EMPC). Attaining higher control performances and reducing energy wasting can be expected by combining these techniques.

Appendix

In Figure 7, the geometric description for the tube and flame is presented.

The view factor of node 2 lying on a cylindrical surface (tube) and node 1 lying on plane work-piece (flame) can be calculated by the following relation [45]:

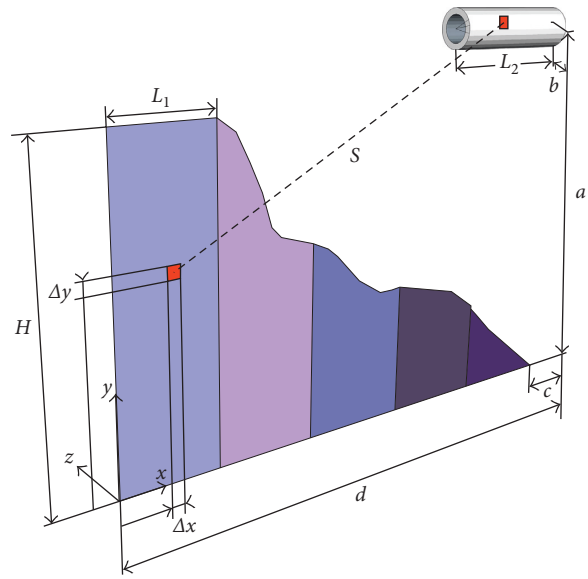

Figure 7: View factor for plane and cylinder shapes.

$$F_{12} = \frac{Sr_{\text{out}}}{S^2 + (y-(H/2))^2}\left(2 - \frac{1}{\pi}\cos^{-1}\left(\frac{\Delta_3}{\Delta_2}\right) + \cos^{-1}\left(\frac{\Delta_6}{\Delta_5}\right) - \frac{(L-x)}{r_{\text{out}}}\left[\frac{\Delta_1}{\sqrt{\Delta_2^2 + 4(L-x)^2 r_{\text{out}}^2}}\cos^{-1}\left(\frac{r_{\text{out}}\Delta_3}{\Delta_2\sqrt{S^2 + (y-(H/2))^2}}\right)\right]\right.$$
$$\left. - \left(\frac{x}{r_{\text{out}}}\right)\frac{\Delta_4}{\sqrt{\Delta_5^2 + 4x^2 r_{\text{out}}^2}}\cos^{-1}\left(\frac{r_{\text{out}}\Delta_6}{\Delta_5\sqrt{S^2 + (y-(H/2))^2}}\right) + \frac{L}{r_{\text{out}}}\cos^{-1}\left(\frac{r_{\text{out}}}{\sqrt{S^2 + (y-(H/2))^2}}\right)\right), \tag{A.1}$$

where S indicates the distance between the center of plane element (flame) and the center of the cylindrical element (tube) that can be calculated as

$$S = \sqrt{(x + 0.5L - d)^2 + (y-a)^2 + z^2}. \tag{A.2}$$

In addition, Δ_is is calculated with respect to the dimensions of the flame and tube as follows:

$$\begin{aligned}
\Delta_1 &= (L-x)^2 + S^2 + \left(y - \frac{H}{2}\right)^2 + r_{\text{out}}^2,\\
\Delta_2 &= (L-x)^2 + S^2 + \left(y - \frac{H}{2}\right)^2 - r_{\text{out}}^2,\\
\Delta_3 &= (L-x)^2 - S^2 - \left(y - \frac{H}{2}\right)^2 + r_{\text{out}}^2,\\
\Delta_4 &= x^2 + S^2 + \left(y - \frac{H}{2}\right)^2 + r_{\text{out}}^2,\\
\Delta_5 &= x^2 + S^2 + \left(y - \frac{H}{2}\right)^2 - r_{\text{out}}^2,\\
\Delta_6 &= x^2 - S^2 - \left(y - \frac{H}{2}\right)^2 + r_{\text{out}}^2.
\end{aligned} \tag{A.3}$$

The overall view factor of the flame for each tube subsection can be obtained by integrating F_{12} into the corresponding region [24]. The length of $L_1 = L_2$ and are equal to the flame width, L. It should be noted that the boundary of integration would change with respect to the position of each zones. We have obtained the following:

$$F = \frac{1}{H\,L}\int_0^H \int_\alpha^\beta F_{12}\, dxdy,$$
$$\alpha = (i-1)\times L,\ \beta = i\times L, \quad i = 1, \ldots, 5. \tag{A.4}$$

View factors were obtained by numerical evaluation of integral equations in MATLAB. Due to symmetric geometry of the firebox, view factors were calculated only for one side, which would considerably reduce computational efforts.

Data Availability

The data used to support the findings of this study are available from the corresponding author upon request.

Conflicts of Interest

The authors declare that they have no conflicts of interest.

References

[1] F. Wildy, *Fired Heater Optimization*, A. P. Instruments, Pittsburgh, PA, USA, 2000.

[2] A. Fuchs, D. R. Lewin, and S. J. Wajc, "Modelling, simulation and control of a crude oil preheating furnace," *Chemical Engineering Science*, vol. 48, no. 4, pp. 661–679, 1993.

[3] J. Varghese and S. Bandyopadhyay, "Fired heater integration into total site and multiple fired heater targeting," *Applied Thermal Engineering*, vol. 42, pp. 111–118, 2012.

[4] X. Wang and D.-Z. Zheng, "Difference control of parallel streams temperatures," *Journal of Process Control*, vol. 15, no. 5, pp. 531–536, 2005.

[5] C. E. Baukal Jr., *The John Zink Hamworthy Combustion Handbook: Volume 1-Fundamentals*, CRC Press, Boca Raton, FL, USA, 2012.

[6] B. Maghbooli, A. Bakhtiari, and H. Najafi, "Correcting improper performance of direct fired heaters," *Chemical Engineering*, vol. 120, pp. 39–46, 2013.

[7] C. E. Baukal Jr., *The John Zink Hamworthy Combustion Handbook: Volume 2-Design and Operations*, CRC Press, Boca Raton, FL, USA, 2013.

[8] Y. Dai, H. Wang, F. Khan, and J. Zhao, "Abnormal situation management for smart chemical process operation," *Current Opinion in Chemical Engineering*, vol. 14, pp. 49–55, 2016.

[9] R. F. Garcia, "Improving heat exchanger supervision using neural networks and rule based techniques," *Expert Systems with Applications*, vol. 39, no. 3, pp. 3012–3021, 2012.

[10] W. Wang, H.-X. Li, and J. Zhang, "A hybrid approach for supervisory control of furnace temperature,," *Control Engineering Practice*, vol. 11, pp. 1325–1334, 2003.

[11] S. Hayes, K. Burton, D. O'Sullivan et al., "Application of expert systems to industrial utility equipment optimization," in *Proceedings of the 14th International Conference for Enhanced Building Operations*, China, Beijing, 2014.

[12] T. Chai, J. Ding, and F. Wu, "Hybrid intelligent control for optimal operation of shaft furnace roasting process," *Control Engineering Practice*, vol. 19, no. 3, pp. 264–275, 2011.

[13] J. M. Molina, P. Isasi, A. Berlanga, and A. Sanchis, "Hydroelectric power plant management relying on neural networks and expert system integration," *Engineering Applications of Artificial Intelligence*, vol. 13, no. 3, pp. 357–369, 2000.

[14] P. Baraldi, M. Librizzi, E. Zio, L. Podofillini, and V. Dang, "Two techniques of sensitivity and uncertainty analysis of fuzzy expert systems," *Expert Systems with Applications*, vol. 36, no. 10, pp. 12461–12471, 2009.

[15] Q. Zhang, D. Okrent, G. Apostolakis, and S. Guarro, "An expert system approach for fault diagnosis to cope with spurious sensor signals and process state uncertainty," *Reliability Engineering and System Safety*, vol. 34, no. 2, pp. 121–142, 1991.

[16] A. Bahadori and H. B. Vuthaluru, "Novel predictive tools for design of radiant and convective sections of direct fired heaters," *Applied Energy*, vol. 87, no. 7, pp. 2194–2202, 2010.

[17] G. Robertson, "Advanced and novel modeling techniques for simulation, optimization and monitoring chemical engineering tasks with refinery and petrochemical unit applications," Ph.D. thesis, The Department of Chemical Engineering, Louisiana State University, Baton Rouge, LA, USA, 2014.

[18] Ł. Śladewski, K. Wojdan, K. Świrski, T. Janda, D. Nabagło, and J. Chachuła, "Optimization of combustion process in coal-fired power plant with utilization of acoustic system for in-furnace temperature measurement," *Applied Thermal Engineering*, vol. 123, pp. 711–720, 2017.

[19] J. W. Wu, M. J. Biggs, and E. J. Hu, "Dynamic model for the optimisation of adsorption-based desalination processes," *Applied Thermal Engineering*, vol. 66, no. 1-2, pp. 464–473, 2014.

[20] V. Meidanshahi, B. Corbett, T. A. Adams, and P. Mhaskar, "Subspace model identification and model predictive control based cost analysis of a semicontinuous distillation process," *Computers and Chemical Engineering*, vol. 103, pp. 39–57, 2017.

[21] F. Friedler, "Process integration, modelling and optimisation for energy saving and pollution reduction," *Applied Thermal Engineering*, vol. 30, no. 16, pp. 2270–2280, 2010.

[22] C. C. Pantelides and J. G. Renfro, "The online use of first-principles models in process operations: review, current status and future needs," *Computers and Chemical Engineering*, vol. 51, pp. 136–148, 2013.

[23] A. G. Marchetti, A. Ferramosca, and A. H. González, "Steady-state target optimization designs for integrating real-time optimization and model predictive control," *Journal of Process Control*, vol. 24, no. 1, pp. 129–145, 2014.

[24] J. Ding, C. Yang, and T. Chai, "Recent progress on data-based optimization for mineral processing plants," *Engineering*, vol. 3, no. 2, pp. 183–187, 2017.

[25] R. Rejowski, V. Shah, C. E. Fontenot, P. de Tarso, and V. E. N. Santos, "Sustain activities for real-time optimization models of ethylene plants," *Computer Aided Chemical Engineering*, vol. 27, pp. 351–356, 2009.

[26] N. Tehlah, P. Kaewpradit, and I. M. Mujtaba, "Artificial neural network based modeling and optimization of refined palm oil process," *Neurocomputing*, vol. 216, pp. 489–501, 2016.

[27] F. N. Osuolale and J. Zhang, "Energy efficiency optimisation for distillation column using artificial neural network models," *Energy*, vol. 106, pp. 562–578, 2016.

[28] C. Damour, M. Benne, B. Grondin-Perez, and J.-P. Chabriat, "Nonlinear predictive control based on artificial neural network model for industrial crystallization," *Journal of Food Engineering*, vol. 99, no. 2, pp. 225–231, 2010.

[29] T. Chai, S. J. Qin, and H. Wang, "Optimal operational control for complex industrial processes," *Annual Reviews in Control*, vol. 38, no. 1, pp. 81–92, 2014.

[30] M. Lawryńczuk, "Online set-point optimisation cooperating with predictive control of a yeast fermentation process: a neural network approach," *Engineering Applications of Artificial Intelligence*, vol. 24, no. 6, pp. 968–982, 2011.

[31] J. Guerrero, A. Guisasola, R. Vilanova, and J. A. Baeza, "Improving the performance of a WWTP control system by model-based setpoint optimisation," *Environmental Modelling and Software*, vol. 26, no. 4, pp. 492–497, 2011.

[32] A. Chaibakhsh, N. Ensansefat, A. Jamali, R. Kouhikamali, and H. Najafi, "Crude oil direct fired furnace model," *Applied Thermal Engineering*, vol. 83, pp. 57–70, 2015.

[33] A. Chaibakhsh, M. Pourbeheshtian, M. Sigaroudi, and H. Najafi, "Modeling and fuzzy control of a crude oil preheating furnace," *Applied Mechanics and Materials*, vol. 229–231, pp. 2370–2374, 2012.

[34] O. Yeniay, "Penalty function methods for constrained optimization with genetic algorithms," *Mathematical and Computational Applications*, vol. 10, no. 1, pp. 45–56, 2005.

[35] X. Liu and R. C. Bansal, "Optimizing combustion process by adaptive tuning technology based on integrated genetic algorithm and computational fluid dynamics," *Energy Conversion and Management*, vol. 56, pp. 53–62, 2012.

[36] M. L. D. Wong and W. K. S. Pao, "A genetic algorithm for optimizing gravity die casting's heat transfer coefficients,," *Expert Systems with Applications*, vol. 38, no. 6, pp. 7076–7080, 2011.

[37] S. Sivanandam and S. Deepa, *Introduction to Genetic Algorithms*, Springer Science & Business Media, Berlin, Germany, 2007.

[38] P. J. Fleming and R. C. Purshouse, "Evolutionary algorithms in control systems engineering: a survey," *Control Engineering Practice*, vol. 10, no. 11, pp. 1223–1241, 2002.

[39] B. Mehrkian, A. Bahar, and A. Chaibakhsh, "Genetic-optimized neuro-fuzzy inference system (GONFIS) in nonlinear system identification," in *Proceedings of the 2011 IEEE International Conference on Control System, Computing and Engineering (ICCSCE)*, pp. 263–268, Penang, Malaysia, November 2011.

[40] L. N. de Castro, E. M. Iyoda, F. J. V. Zuben, and R. Gudwin, "Feedforward neural network initialization: an evolutionary approach," in *Proceedings of the 5th Brazilian Symposium on Neural Networks (Cat. No. 98EX209)*, pp. 43–48, Porto Alegre, Brazil, 1998.

[41] S. A. Kalogirou, "Artificial intelligence for the modeling and control of combustion processes: a review," *Progress in Energy and Combustion Science*, vol. 29, no. 6, pp. 515–566, 2003.

[42] E. M. Azoff, *Neural Network Time Series Forecasting of Financial Markets*, John Wiley & Sons, Inc., Hoboken, NJ, USA, 1994.

[43] D. V. R. Fontoura, E. M. Matos, and J. R. Nunhez, "A three-dimensional two-phase flow model with phase change inside a tube of petrochemical pre-heaters," *Fuel*, vol. 110, pp. 196–203, 2013.

[44] M. R. J. Nasr and M. M. Givi, "Modeling of crude oil fouling in preheat exchangers of refinery distillation units," *Applied Thermal Engineering*, vol. 26, no. 14-15, pp. 1572–1577, 2006.

[45] J. Stevenson and J. Grafton, "Radiation heat transfer analysis for space vehicles," Report SID-61-91, North American Aviation, San Diego, CA, USA, 1961.